arXiv:1102.2179v1 [cond-mat.str-el] 10 Feb 2011

Synthesis and Characterization of Single Crystal Samples of Spin-$\frac{1}{2}$ Kagome Lattice Antiferromagnets in the Zn-Paratacamite Family $Zn_xCu_{4-x}(OH)_6Cl_2$

T.H. Han[1,‡], J. S. Helton[1,2], S. Chu[3], A. Prodi[1,†], D. K. Singh[2,4],
C. Mazzoli[5], P. Müller[6], D. G. Nocera[6], and Y. S. Lee[1,‡]
[1]*Department of Physics, Massachusetts Institute of Technology, Cambridge, Massachusetts 02139, USA*
[2]*NIST Center for Neutron Research, Gaithersburg, Maryland 20899, USA*
[3]*Center for Materials Science and Engineering, Massachusetts Institute of Technology, Cambridge, Massachusetts 02139, USA*
[4]*Department of Materials Science and Engineering,*
University of Maryland, College Park, Maryland 20742, USA
[5]*European Synchrotron Radiation Facility, 38043 Grenoble, France and*
[6]*Department of Chemistry, Massachusetts Institute of Technology, Cambridge, Massachusetts 02139, USA*
(Dated: January 12, 2013)

The Zn-paratacamite family, $Zn_xCu_{4-x}(OH)_6Cl_2$ for $x \geq 0.33$, is an ideal system for studying spin-$\frac{1}{2}$ frustrated magnetism in the form of antiferromagnetic Cu^{2+} kagome planes. Here we report a new synthesis method by which high quality millimeter-sized single crystals of Zn-paratacamite have been produced. These crystals have been characterized by metal analysis, x-ray diffraction, neutron diffraction, and thermodynamic measurements. The $x = 1$ member of the series displays a magnetic susceptibility that is slightly anisotropic at high temperatures with $\chi_c > \chi_{ab}$. Neutron and synchrotron x-ray diffraction experiments confirm the quality of these $x = 1$ single crystals and indicate no obvious structural transition down to temperatures of $T = 2$ K.

PACS numbers: 81.10.-h, 75.50.Ee, 61.05.cp

Geometrically frustrated magnetism[1,2] is a forefront area of research in condensed matter physics, as such systems offer a unique terrain in which to search for novel magnetic ground states. The spin-$\frac{1}{2}$ nearest-neighbor Heisenberg antiferromagnet on the kagome lattice, which consists of corner sharing triangles, is a particulary promising system in which to search for unique quantum phases including the "resonating valence bond" (RVB) state proposed by Anderson[3] or other quantum spin liquid states. A broad theoretical and numerical consensus has emerged that the ground state of this system is not magnetically ordered[4–7], with a variety of proposed ground states including gapped spin liquids[8], gapless spin liquids[9,10], and valence bond solid (VBS) states[11,12]. However, experimental investigation on this system has long been hampered by the fact that most early realizations of the kagome lattice antiferromagnet feature either large spins or structural distortions.

The material $ZnCu_3(OH)_6Cl_2$[13,14] is among the best realizations of a spin-$\frac{1}{2}$ kagome lattice antiferromagnet yet synthesized. This material is a member of the Zn-paratacamite family $Zn_xCu_{4-x}(OH)_6Cl_2$ with $x = 1$. With lattice parameters $a = b = 6.83$ Å and $c = 14.05$ Å, $ZnCu_3(OH)_6Cl_2$ is rhombohedral (trigonal setting) and consists of kagome lattice planes of spin-$\frac{1}{2}$ Cu^{2+} ions separated by layers of non-magnetic Zn^{2+} ions as shown in Fig.1(a). Measurements on powder samples[15] have found no sign of long range order or spin freezing down to temperatures of 50 mK[16–18], despite a strong antiferromagnetic superexchange interaction of $J \approx 17$ meV and a Curie-Weiss temperature of $\Theta_{CW} = -300 \pm 20$ K. There is no evidence of a spin gap down to at least J/200[16,19,20]. The most significant deviations of this material from the idealized model are likely the presence of about 5% weakly-coupled Cu^{2+} ions lying on out-of-plane metallic sites, which may be responsible for the Curie-like susceptibility at low temperatures, and Dzyaloshinksii-Moriya or exchange anisotropy interactions. Recent anomalous x-ray diffraction measurements indicate that dilution of the kagome plane sites with Zn ions is not significant[21]. Studies on Zn-paratacamite samples[17,22,23] with $x < 1$ can be useful in determining the effect of any out-of-plane impurities that might be present even in the nominal $x = 1$ samples, as well as serving as model systems for weakly coupled kagome planes.

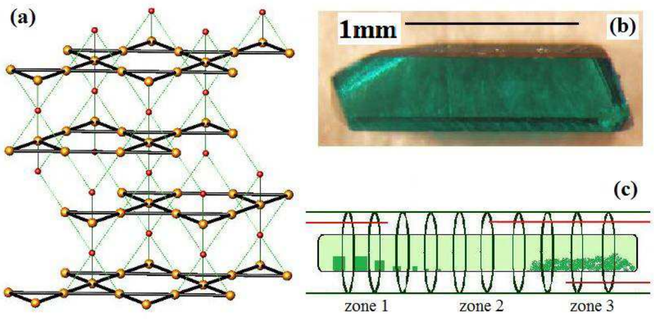

FIG. 1: (color online) (a) Structure of $ZnCu_3(OH)_6Cl_2$ with only Cu^{2+}(large brown spheres) and Zn^{2+}(small red spheres) displayed. The Cu-Cu bonds (thick black solid lines) are all equivalent as are the Cu-Zn bonds (thin green dotted lines). (b) A single crystal sample of $ZnCu_3(OH)_6Cl_2$. (c) A schematic of three zone furnaces. The red bars indicate the positions of the thermocouples.

Previous studies of Zn-paratacamite have utilized powder samples grown by hydrothermal methods. The failure of these methods to produce large single crystals has been ascribed partly to the low decomposition temperature of $ZnCu_3(OH)_6Cl_2$. However, the primary reason for the lack of single crystal synthesis is likely the fact that the reported synthesis[14] produces bubbles of CO_2, resulting in an unstable crystallization environment. Further understanding of the spin behavior of $ZnCu_3(OH)_6Cl_2$, and further insight into the ground state of the spin-$\frac{1}{2}$ kagome lattice antiferromagnet, will require studies on single crystal samples. Here we report a new synthesis method by which high quality millimeter-sized single crystals have been successfully produced. These samples have been characterized by a variety of measurements.

Single crystal samples of Zn-paratacamite, $Zn_xCu_{4-x}(OH)_6Cl_2$, were grown hydrothermally in furnaces that were setup similarly to those used to grow small single crystal samples of the atacamite family[24] and $Mg_xCu_{4-x}(OH)_6Cl_2$[25]. Here, starting materials of CuO, $ZnCl_2$, and H_2O, in amounts listed in Table I, were charged into a fused quartz tube (ID 6 mm, OD 13 mm for x=0.8 and 1.0 or ID 9 mm, OD 15 mm for x=0.9). The quartz tube was sealed after purging air with a mechanical pump. The sealed quartz tube was prereacted for two days in a box furnace at 185 °C. After prereaction, a green-blue microcrystalline powder was formed. Powder x-ray diffraction measurements of this product have indicated the presence of $Zn_xCu_{4-x}(OH)_6Cl_2$. This shows successful synthesis by the reaction

$$(4-x)\mathrm{CuO} + \mathrm{ZnCl_2} + 3\mathrm{H_2O} \rightarrow \mathrm{Zn}_x\mathrm{Cu}_{4-x}(\mathrm{OH})_6\mathrm{Cl_2} + (1-x)\mathrm{ZnO}. \quad (1)$$

This synthesis without the production of CO_2 suggests the possibility of an environment stable enough for single crystal growth.

Millimeter-sized single crystals were synthesized through a recrystallization process in a three-zone gradient tube furnace. A schematic of such a furnace is shown in Fig. 1(c). The sealed, prereacted quartz tubes were placed horizontally into the furnace at room temperature. The furnace temperature was isotropically increased to a fixed temperature, ranging from 165 °C to 180 °C in various reactions. The temperature of the cold end was then slowly lowered. The sample and all growth parameters were undisturbed for roughly 20 weeks until large crystals were formed at the cold end. In the region where the crystals nucleated and grew, the temperature gradient was measured to be approximately 1 °C/cm. At the end of the synthesis, the sample tubes were cooled down to room temperature at 1 °C/min. Crystals were then rinsed with deionized water, dried in air and kept in a desiccator for storage. No decomposition of the crystals has been observed in air, water, or acetone. Precise control of the starting concentrations of CuO and $ZnCl_2$ allows for synthesis of samples with variable Zn concentration, x. Data on crystals with $x = 0.8$, 0.9, and 1.0 are shown in Table I. More syntheses than listed in Table I were performed with $ZnCl_2$ to CuO molar ratios ranging from 2 to 10 and with $ZnCl_2$ to H_2O concentrations ranging from 1.2 mmol/ml to 7.7 mmol/ml. However, the x values of the final products were fairly stable over this range of starting concentrations. At a fixed $ZnCl_2$ to CuO ratio, the x value of the product increased with increasing $ZnCl_2$ concentration, from an x value of 0.8 with a $ZnCl_2$ concentration of 1.2 mmol/ml to an x value of 1.0 with a $ZnCl_2$ concentration of 2.8 mmol/ml. Products with an x value of 1.0 were also obtained for starting $ZnCl_2$ concentrations up to 5.6 mmol/ml, while even higher $ZnCl_2$ concentrations resulted in a slight lowering of x. This diminishment of x with very high $ZnCl_2$ concentrations is likely due to a more acidic pH in those reactions which dissolves more CuO. The $ZnCl_2$ to CuO molar ratio of the starting products had no obvious effect on the x values of the product over the range of syntheses performed. The compositions of the crystals were measured by metal analysis taken with an inductively coupled plasma atomic emission spectrometer (ICP-AES) with an error of ±0.04 on x. Standards were prepared from commercially purchased solutions from Sigma-Aldrich, specific for ICP-AES measurements and designated as Trace SELECT grade or better. Five to ten well rinsed small single crystals from each synthesis tube, approximately 0.1 mg each, were dissolved into 2% w/w nitric acid for measurement. Unlike powder samples, the ease to rinse single crystals dramatically reduced the ambiguity from possible chemical contamination. The relative amounts of Cu and Zn determined from ICP metal analysis were used to calculate the values of x listed in Table I. Our nominal $x = 1$ sample has previously been determined to have structural composition $(Zn_{0.85}Cu_{0.15})Cu_3(OH)_6Cl_2$ via anomalous x-ray scattering.[21] Here, the kagome planes are fully occupied with Cu, and anti-site disorder[26,27] with Zn on the Cu kagome site is not apparent.

TABLE I: Growth and crystallography data. All samples have rhombohedral crystal system in R$\bar{3}$m space group (α=β=90°, γ=120°. Single crystal x-ray diffraction was performed at T = 100 K and refined by full-matrix least-squares on F^2 with goodness-of-fit (GOF) listed. Curie-Weiss temperatures were determined from high temperature susceptibilities.

	$x = 0.8$	$x = 0.9$	$x = 1.0$
Starting materials (g)	CuO (0.130) $ZnCl_2$ (0.686) H_2O (4.0 ml)	CuO (0.346) $ZnCl_2$ (2.985) H_2O (10.0 ml)	CuO (0.235) $ZnCl_2$ (2.015) H_2O (4.5 ml)
Hot zone temp.	165 °C	165 °C	180 °C
a	6.8300(13) Å	6.8345(9) Å	6.8332(12) Å
b	6.8300(13) Å	6.8345(9) Å	6.8332(12) Å
c	14.029(3) Å	14.0538(19) Å	14.066(2) Å
Volume (Å^3)	566.77(19)	568.51(13)	568.80(17)
Density, ρ	3.765 g/cm^3	3.759 g/cm^3	3.755 g/cm^3
total reflections	2673	3718	5908
indep reflections	238	225	240
GOF	1.275	1.264	1.237
Θ_{CW}	-266(10) K	-290(10) K	-296(10) K

Single crystal x-ray diffraction was performed on a three-circle diffractometer coupled to a CCD detector. All samples were refined in the rhombohedral space group R$\bar{3}$m (trigonal setting) and with lattice constants consistent with previous reports. The largest (1 to 10 mm^3) crystals typically grow as a bar-shape similar to the crystal shown in Fig. 1(b). From x-ray diffraction on more than 30 crystals, all of the side long faces were indexed as (1 0 1) (the faces were normal to the (1 0 1) reciprocal lattice vector). Some of the smaller ($<$ 0.5 mm^3) crystals were octahedrally shaped, with all eight faces indexed as (1 0 1). Based on these observations, we propose the following growth process: during the early stage of crystallization, primitive micrometer-sized crystals form as twelve-faced polyhedra due to the symmetry of the (1 0 1) directions. As the crystals grow larger in size, eight of the twelve (1 0 1) faces, possibly due to the specific local hydrodynamic condition, grow faster which transforms the crystals into larger, sub-millimeter octahedra. Eventually, four of these eight (1 0 1) faces form the four large side faces of millimeter-sized bar-shaped crystals.

The single crystal samples obtained by this synthesis were characterized by a variety of methods. Single crystal susceptibility measurements of an $x = 1$ sample were performed on a SQUID magnetometer (Quantum Design) using a 55.5 mg sample (different from the one in Fig. 1(b)) with an almost cubic shape (2.3 mm × 2.5 mm × 2.7 mm). Figure. 2(a) shows the bulk susceptibility, $\chi \equiv M/H$, as a function of temperature. The susceptibility of the crystal closely follows that measured on a powder sample with $x = 1$ (also plotted), which confirms that the stoichiometry and homogeneity of the single crystals match that of previously measured powders. The inset of panel (a) shows the specific heat of an $x = 1$ single crystal measured at $\mu_0 H = 0$ T and compared with data from a powder sample. Again, the two curves show good agreement, where the higher quality of single crystal measurements is likely due to the better thermal contact with the sample holder. In Fig. 2(b), we show the magnetic susceptibility plotted as MT/H, with an applied magnetic field of $\mu_0 H = 1$ T aligned along the different crystallographic axes, (χ_c) and(χ_{ab}). Powder data are also plotted (χ_{powder}) for comparison. The calculated powder averaged value of the single crystal data ($\chi_{av} \equiv \frac{2}{3}\chi_{ab} + \frac{1}{3}\chi_c$) is indicated by the solid line. As expected, the calculated χ_{av} and χ_{powder} show good agreement. At high temperatures, the single crystal data show clear magnetic anisotropy with $\chi_c > \chi_{ab}$. The inset to panel (b) shows the high temperature (80 K and 300 K) magnetization; the anisotropy is field independent, with M_c/M_{ab} a constant up to $\mu_0 H = 5$ T. This high temperature anisotropy is consistent with the qualitative results obtained from powder samples that were partially oriented in a magnetic field[28] and μSR measurement on single crystal samples[29]. The anisotropy of the magnetization should play a role in elucidating the effects that the Dzyaloshinskii-Moriya interaction, exchange anisotropy, or out-of-plane impurities have on the low temperature physics of the material[30,31]. The bulk susceptibility of crystals with $x = 0.8$ and 0.9 are also consistent with powder samples (not shown). A detailed study of the susceptibility and specific heat of samples with different x-values is a topic of ongoing investigation.

Among the various predicted ground states for the spin-$\frac{1}{2}$ nearest-neightbor Heisenberg kagome antiferromagnet, several theoretical studies have suggested a 36-site valence bond solid[11,12]. This proposed ground state features a $\sqrt{12} \times \sqrt{12}$ enlargement of the unit cell, with the 36 spin sites paired into 18 nearest-neighbor dimer singlets, where 6 dimers lie around a central pinwheel configuration while another 6 lie around hexagons. The two possible coverings of the pinwheel are degenerate to high order, while sets of three dimers can resonate around a perfect hexagon[11]. The other 6 dimers are presumed to be static. It has been suggested[32] that a VBS order might lead to a slight structural distortion in which the distance between two magnetic ions paired in a singlet is diminished. Such a distortion, if large enough, could in principle be measured in a synchrotron x-ray experiment.

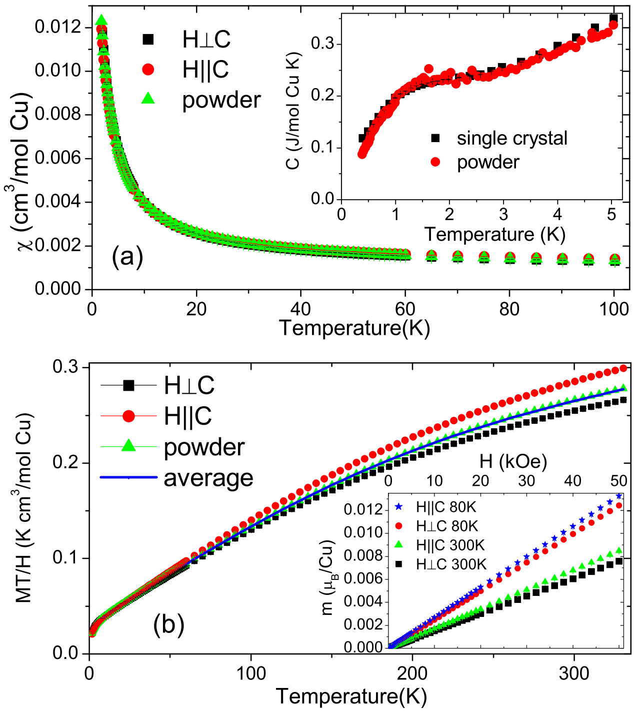

FIG. 2: (color online) (a) The bulk susceptibility, M/H, of an $x = 1$ single crystal as a function of temperature. Also plotted are results from powder samples. Inset: Low temperature specific heat of an $x = 1$ single crystal compared with powder data (with $H = 0$). (b) Plots of MT/H versus temperature, showing the anisotropy $\chi_c > \chi_{ab}$ at high temperatures. Inset: M versus H curves at 80 K and 300 K along different directions.

We performed diffraction measurements on our single crystals with $x = 1$. Figure. 3(a) shows a θ-scan through the (1 1 0) Bragg reflection measured with neutron diffraction using the SPINS spectrometer at the NIST Center for Neutron Research. The width of the scan of 0.5°, which is resolution-limited, attests to the crystal homogeneity. A high-resolution x-ray diffraction experiment on a small $x = 1.0$ single crystal was performed on the ID20 beamline of the European Synchrotron Radiation Facility (ESRF). The scattering was performed in reflection geometry with the (1 0 1) reflection roughly perpendicular to the mount, with x-rays of energy of 8.979 keV ($\lambda = 1.381$ Å). The sample was cooled with a closed-cycle displex and was mounted on a four-circle goniometer. The measurements indicate that the sample remains in space group R$\bar{3}$m down to the lowest measured temperature $T \simeq 2$ K. The high x-ray flux available at a synchrotron is ideal to look for very subtle superlattice reflections that would arise if a VBS ground state resulted in a structural distortion. The 36-site VBS would lead to an enlarged unit cell that is a factor of $\sqrt{12}$ longer on each side and rotated 90° from the original unit cell. We searched for the superlattice reflections along the high-symmetry (1 1 0) direction between the (4 0 4) and (5 1 4) peaks. This scan, shown in Fig. 3(b), showed no observable superlattice peaks above the background. The only scattering features in this range were very weak powder peaks (roughly 250,000 times weaker than the strongest lattice reflections). These peaks were confirmed to arise from powder through θ-scans; they also displayed no temperature dependence and were somewhat broader than resolution. Contamination from these powder peaks, although exceptionally weak, is likely the limiting factor in setting an upper bound on the possibility of any su-

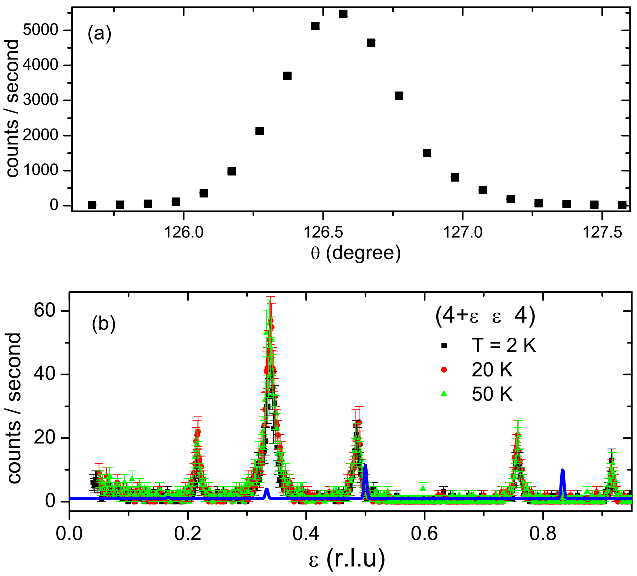

FIG. 3: (color online) (a) Neutron diffraction θ-scan through the (1 1 0) Bragg reflection of an $x = 1$ single crystal measured with the SPINS neutron spectrometer. (b) Synchrotron x-ray diffraction intensity of a scan along the $(4{+}\epsilon\ \epsilon\ 4)$ direction at three temperatures, 2 K, 20 K and 50 K. The extremely weak peaks observed in this range arise from powder contamination and have no temperature dependence. The lines are a simulation of the superlattice peaks arising from a 36-site valence bond solid with a 1% reduction in the bond length of the static dimer pairs, as discussed in the text.

perlattice reflections. The blue lines in Fig. 3(b) are a calculation of the superlattice peaks expected if the copper ions making up the 6 static dimer pairs per supercell (dimers that are in neither a pinwheel nor a perfect hexagon) were to move toward one another such that the Cu-Cu distance was reduced by 1%. It was assumed that the centering of the enlarged unit cells on adjacent kagome planes is random, so that the superlattice peaks will actually be rods of scattering parallel to c. The lack of observed superlattice peaks at the expected positions indicates that any structural distortions due to this proposed supercell are below the 1% level. Note that the intensity of the superlattice peaks is proportional to the displacement squared in the limit of small displacement. Additional mesh scans (not shown) found no evidence of other superlattice peaks, as might arise from VBS states with different enlarged unit cells[32]. Of course, this experiment cannot rule out the presence of a VBS ground state that results in very little or no structural change.

In summary, high quality single crystals of $\mathrm{Zn}_x\mathrm{Cu}_{4-x}(\mathrm{OH})_6\mathrm{Cl}_2$ have been synthesized and characterized. The bulk properties of $x = 1$ single crystals are consistent with the previously published powder results. The susceptibility measured along different crystallographic directions shows clear anisotropy. This indicates the presence of additional terms in the spin Hamiltonian, such as a small Dzyaloshinskii-Moriya interaction or exchange anisotropy. Synchrotron x-ray scattering experiments did not show evidence for the emergence of superlattice peaks at low temperatures. Hence, any possible lattice distortions associated with a valence bond solid are subtle, if they exist. Clearly, further measurements on these single crystal samples should help reveal the physics of the $S = 1/2$ kagome ground-state.

We thank E.A. Nytko, D. Freedman, and T. McQueen for useful discussions. The work at MIT was supported by the Department of Energy (DOE) under Grant No. DE-FG02-07ER46134. This work utilized facilities supported in part by the National Science Foundation under Agreement No. DMR-0454672.

[†] Present address: Niels Bohr Institute, University of Copenhagen, Denmark
[‡] email: tianheng@alum.mit.edu, younglee@mit.edu

---

[1] A. P. Ramirez, Annu. Rev. Mater. Sci. **24**, 453 (1994).
[2] G. Misguich *et al.*, in *Frustrated Spin Systems*, edited by H. T. Diep (World Scientific, Singapore, 2004).
[3] P. W. Anderson, Mat. Res. Bull. **8**, 153 (1973).
[4] C. Zeng *et al.*, Phys. Rev. B **42**, 8436 (1990).
[5] J. B. Marston *et al.*, J. Appl. Phys. **69**, 5962 (1991).
[6] R. R. P. Singh *et al.*, Phys. Rev. Lett. **68**, 1766 (1992).
[7] S. Sachdev, Phys. Rev. B **45**, 12377 (1992).
[8] C. Waldtmann *et al.*, Eur. Phys. J. B **2**, 501 (1998).
[9] Y. Ran *et al.*, Phys. Rev. Lett. **98**, 117205 (2007).
[10] S. Ryu *et al.*, Phys. Rev. B **75**, 184406 (2007).
[11] R. R. P. Singh *et al.*, Phys. Rev. B **76**, 180407(R) (2007).
[12] P. Nikolic *et al.*, Phys. Rev. B **68**, 214415 (2003).
[13] R. S. W. Braithwaite *et al.*, Min. Mag. **68**, 527 (2004).
[14] M. P. Shores *et al.*, J. Am. Chem. Soc. **127**, 13462 (2005).
[15] P. Mendels *et al.*, J. Phys. Soc. Japan **79**, 011001 (2010).
[16] J. S. Helton *et al.*, Phys. Rev. Lett. **98**, 107204 (2007).
[17] P. Mendels *et al.*, Phys. Rev. Lett. **98**, 077204 (2007).
[18] O. Ofer *et al.* (2006), arXiv:cond-mat/0610540v2.
[19] A. Olariu *et al.*, Phys. Rev. Lett. **100**, 087202 (2008).
[20] D. Wulferding *et al.*, Phys. Rev. B **82**, 144412 (2010).
[21] D. E. Freedman *et al.*, J. Am. Chem. Soc. **132**, 16185 (2010).
[22] S.-H. Lee *et al.*, Nat. Mater. **6**, 853 (2007).
[23] M. A. de Vries *et al.*, Phys. Rev. Lett. **100**, 157205 (2008).
[24] S. Chu, *et al.,* unpublished.
[25] S. Chu *et al.*, J. Am. Chem. Soc. **132**, 5570 (2010).
[26] R.R.P.Singh, Phys. Rev. Lett. **104**, 177203 (2010).
[27] M. A. de Vries *et al.*, Phys. Rev. Lett. **103**, 237201 (2009).
[28] O. Ofer *et al.*, Phys. Rev. B **79**, 134424 (2009).
[29] O. Ofer *et al.* (2010), arXiv:cond-mat/1012.3511v1.
[30] M. Rigol *et al.*, Phys. Rev. Lett. **98**, 207204 (2007).
[31] M. Rigol *et al.*, Phys. Rev. B **76**, 184403 (2007).
[32] M. J. Lawler *et al.*, Phys. Rev. Lett. **100**, 187201 (2008).